International Journal of Biological Macromolecules 149 (2020) 1130–1138

Contents lists available at ScienceDirect

International Journal of Biological Macromolecules

journal homepage: http://www.elsevier.com/locate/ijbiomac

Laccase immobilized polyaniline/magnetic graphene composite electrode for detecting hydroquinone

Congqiang Lou [a], Tao Jing [a,*], Juying Zhou [b,e], Jingzhi Tian [a], Yongjie Zheng [a], Chao Wang [a], Zhiyuan Zhao [a], Jing Lin [c,*], Hu Liu [d], Chunqi Zhao [a], Zhanhu Guo [e,*]

[a] School of Chemistry and Chemical Engineering, Qiqihar University, Qiqihar 161000, China
[b] School of Chemistry and Chemical Engineering, Guangxi University for Nationalities, Nanning 530006, China
[c] School of Chemistry and Chemical Engineering, Guangzhou University, Guangzhou 510006, China
[d] Key Laboratory of Materials Processing and Mold (Zhengzhou University), Ministry of Education, National Engineering Research Center for Advanced Polymer Processing Technology, Zhengzhou University, Zhengzhou, China
[e] Integrated Composites Lab (ICL), Department of Chemical & Biomolecular Engineering, University of Tennessee, Knoxville, TN 37996, USA

ARTICLE INFO

Article history:
Received 14 November 2019
Received in revised form 15 January 2020
Accepted 24 January 2020
Available online 27 January 2020

Keywords:
Graphene
Laccase
Sensor

ABSTRACT

Magnetic graphene nanocomposites were prepared by hydrothermal synthesis, and aniline polymerization was initiated by magnetic graphene. These polyaniline/magnetic graphene (PANI/MG) composites were used to immobilize laccase to construct biosensors. Scanning electron microscopy (SEM), transmission electron microscopy (TEM), X-ray diffraction (XRD) and infrared spectroscopy (IR) were used to characterize these composites. Cyclic voltammetry and chronoamperometry technique were used to test the electrical properties of the constructed polyaniline/magnetic graphene laccase modified electrode. The results show that the polyaniline/magnetic graphene immobilizing laccase modified electrode exhibited superior electrical properties, including high sensitivity, detection limit and linear range. The hydroquinone was used as an analytical and detection probe. The selectivity was 0.03639 A/(mol/L), the linear range was 0.4–337.2 μmol/L, and the detection limit was 2.94 μM (signal/noise = 3, minimum identification value of effective signal). The biosensor can reach the conditions for detecting the actual water sample.

1. Introduction

Phenolic compounds are one of the common chemical raw materials. Hydroquinone is one of the common phenolic compounds and is widely used in chemical products such as industry, medicine, and pesticides [1–3]. However, due to its high toxicity and refractory nature, it will cause damage to the environment and will affect the ecological balance and human health [4–6]. Therefore, the detection of hydroquinone is particularly important. At present, traditional detecting methods for phenols include spectrophotometry, high performance liquid chromatography, gas chromatography and other detection methods [7–9]. However, these conventional methods are complicated and time-consuming, require expensive instruments and have a low sensitivity. Therefore, a rapid and efficient method for detecting hydroquinone is the focus of research. Recent years, electrochemical methods have attracted attention because of their fast and efficient characteristics [10–12]. In the detection of phenolic compounds, electrochemical biosensors can quickly and sensitively detect phenolic substances in water, and have the advantages of low cost, good sensitivity, etc., and have broad prospects, which are of great concern to researchers [13–16]. Graphene is a new type of two-dimensional carbon nanomaterial [17–24]. Its unique sheet structure makes it have excellent electrical conductivity [25–30] and high theoretical specific surface area [31–34], and it has a wide range of applications in the electrochemical direction [35–38]. Graphene has obvious disadvantages in the role of van der Waals force between sheets, and the occurred aggregation affects the application and development of graphene [39–41]. The combination of graphene and nanoparticles can reduce accumulation, partially solving this problem and making it more widely used in the electrochemical applications.

Fe_3O_4 nanoparticles (NPs) are rich in nature and have excellent redox activity, environmentally friendly, low cost, and have received extensive attention and applications [42–48]. The surface of Fe_3O_4 NPs is rough, and the uneven atomic step is advantageous for increasing the area of chemical reaction. In addition, because of high electrical conductivity, excellent biocompatibility, and no toxic side effects, Fe_3O_4 NPs are used in the biosensor to immobilize the enzyme to realize direct

* Corresponding authors.
E-mail addresses: jtkr@163.com (T. Jing), linjing@gzhu.edu.cn (J. Lin), zguo10@utk.edu, nanomaterials2000@gmail.com (Z. Guo).

https://doi.org/10.1016/j.ijbiomac.2020.01.248
0141-8130/

electron transfer of the enzyme to enhance the catalytic activity. In particular, magnetic particles of Fe_3O_4 NPs are considered to be good applications for immobilizing biomolecules due to their superparamagnetic properties and unique advantages of bridging catalysts and substrates. Polyaniline (PANI) is a kind of common conductive polymer with excellent processing performance, simple preparation process and good biocompatibility [49–58]. It has the characteristics of directing electron transfer on the surface of the enzyme electrode and similar excellent electrical conductivity to metals, making it widely studied for biosensors [59–62].

Laccase (Lac) is a multi-copper polyphenol oxidase that can effectively catalyzes the oxidation of many phenolic compounds, accompanied by the reduction of oxygen to water. Due to its highly efficient biological catalysis, laccase is currently widely used in environmental wastewater treatment and microbial conversion of natural products. In addition, laccase-based biosensors are used to determine the phenols in foods, environment and body fluids [63–66].

In this paper, a laccase biosensor was prepared from PANI/MG composites to detect hydroquinone in water. The composites were characterized by electron microscopy, X-ray diffraction, infrared spectroscopy, etc. The electrochemical properties of the modified electrodes were analyzed and the biosensors were evaluated.

2. Material and methods

2.1. Materials and instruments

Aniline (analytically pure) was supplied by Tianjin Kemi Chemical Reagent Co., Ltd. (Tianjing, China). Natural flake graphite was obtained from Qingdao Jinrilai Graphite Co., Ltd. (Qingdao, China). Laccase was purchased from Cool Biotechnology Co., Ltd. (Fuyang, China). Other reagents were of analytical grade, and the solution was prepared with ultrapure water. Nafion (5% *w*/w) was supplied from E.I. DuPont Company.

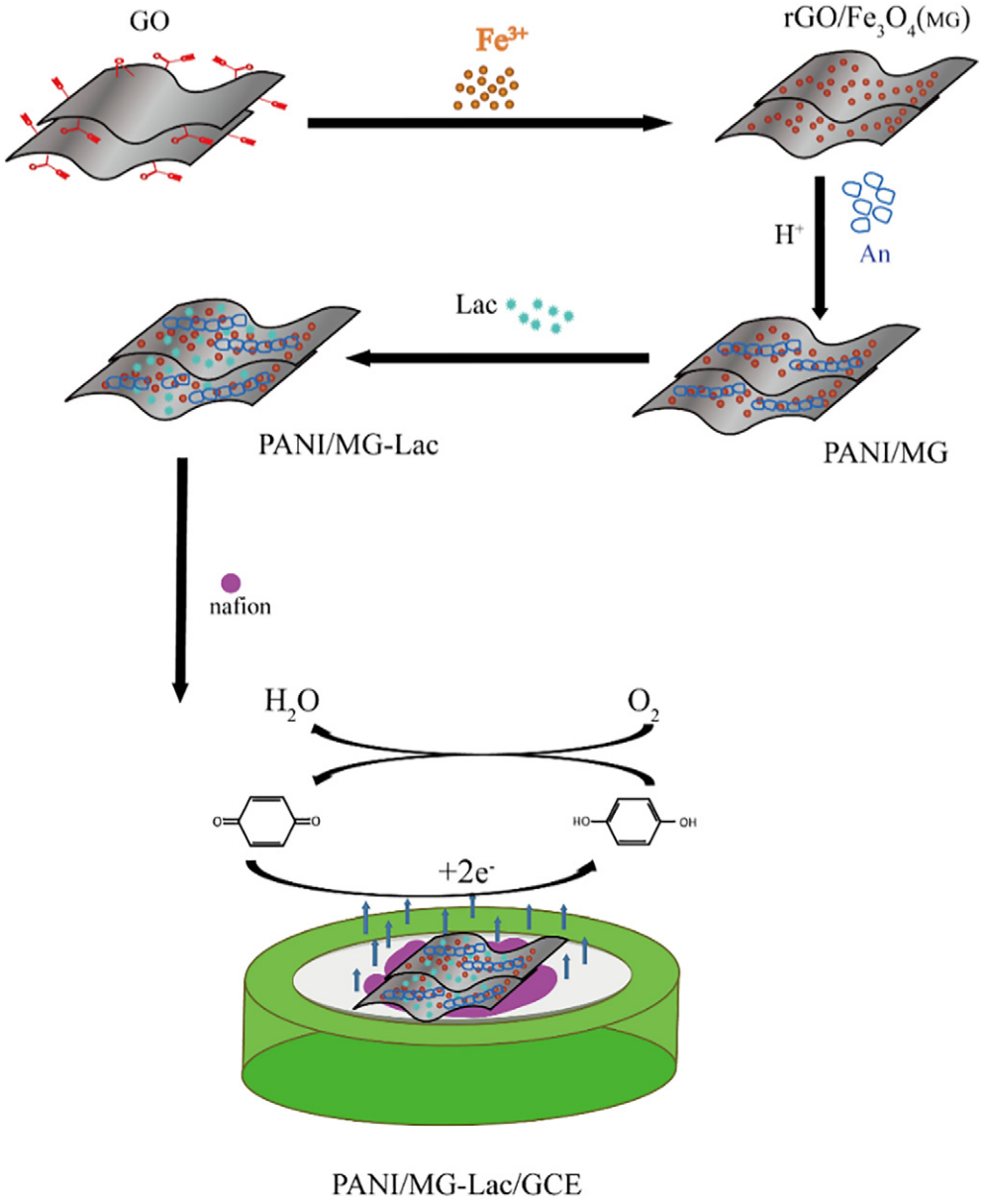

Scheme 1. Schematic of the fabrication of polyaniline/magnetic graphene-Lac-GCE and laccase catalyzed oxidation of hydroquinone with its subsequent electrochemical reduction on the GCE.

A CHI660C electrochemical workstation (Shanghai Chenhua Instrument Co., Ltd.) was employed. The morphologies were characterized by scanning electron microscope (HITICHA S-4300,Tokyo, Japan) and transmission electron microscope (HITICHA S-7650, Tokyo, Japan). The chemical components were analyzed by Powder D8 Advance X-ray diffraction (XRD, Bruker AXS D8). The surface chemistry of materials was examined by Fourier transform infrared spectroscopy (Nicolet380 FT-IR spectrometer, Thermo Fisher Scientific) based on KBr tablet from 500 to 4000 cm^{-1}.

2.2. Preparation of magnetic graphene (MG)

Graphite oxide (GO) was prepared according to the modified Hummers method [67]. Briefly, 2 mg/mL graphite oxide (80 mg)-ethylene glycol (40 mL) solution was treated by ultrasonic stripping for 60 min to obtain a brown dispersion of graphene oxide. 0.5 g of $FeCl_3 \cdot 6H_2O$ was dissolved in the above graphene oxide solution, and the mixed solution was constantly stirred for 2 h. Then, 3.6 g of crystalline sodium acetate and 1.0 g of polyethylene glycol were added and stirred for 30 min for preventing the agglomeration. The mixture was then transferred to a stainless steel autoclave and heated at 200 °C for 16 h. The black product was washed several times with ethanol by centrifugation and dried at 50 °C in a vacuum oven.

2.3. Preparation of polyaniline/magnetic graphene

60 mg magnetic graphene was dissolved in 40 mL 1 mol/L HCl solution and ultrasonically dispersed. The solution was stirred at 200 rpm/min using a stirrer, and then 50 mg of aniline was added and stirred for 30 min to adsorb on the magnetic graphene. Ammonium persulfate with a molar ratio of 0.1:1 to aniline was slowly added dropwise to the above solution. After 10 min, the reaction was carried out for 4 h. After that, it was washed with water and absolute ethanol to neutrality, and transferred for freeze-drying. The composites were dried for 48 h. The polyaniline/magnetic graphene composites were prepared for use. At the same time, the composites having different mass ratios (MG: PANI = 0.1:1, 0.1:2, and 0.1:2.5) were prepared according to the above conditions.

2.4. Fabrication of biosensors

The polyaniline/magnetic graphene composites were dispersed in a 1.5% nafion solution by sonication for 15 min to obtain a 3 mg/mL polyaniline/magnetic graphene solution. Then, laccase was added to adjust the concentration to 3 mg/mL, stirred for 30 min, and then adsorbed at 4 °C for 48 h. 8 μL of the dispensed solution was applied dropwise onto the electrode and dried in a freezer at 4 °C and designated as PANI/MG-Lac-GCE. According to the same preparation process, the bare electrode, Lac-GCE and MG-Lac-GCE were prepared for comparison (Scheme 1).

2.5. Electrochemical performance

A three-electrode system was used, i.e., modified glassy carbon electrode (GCE) as working electrode, Pt electrode as counter electrode, and saturated Ag/AgCl electrode as reference electrode. Cyclic voltammetry technology was used evaluate the working electrodes by observing the relationship between potential and current, and the peak value of the current. The experimental voltages of the cyclic voltammetry technology were: −0.2–0.8 V in buffer solution and −0.4–1.0 V in buffer solution containing hydroquinone. The chronoamperometry technology was used to evaluate and analyze the biosensors by recording the

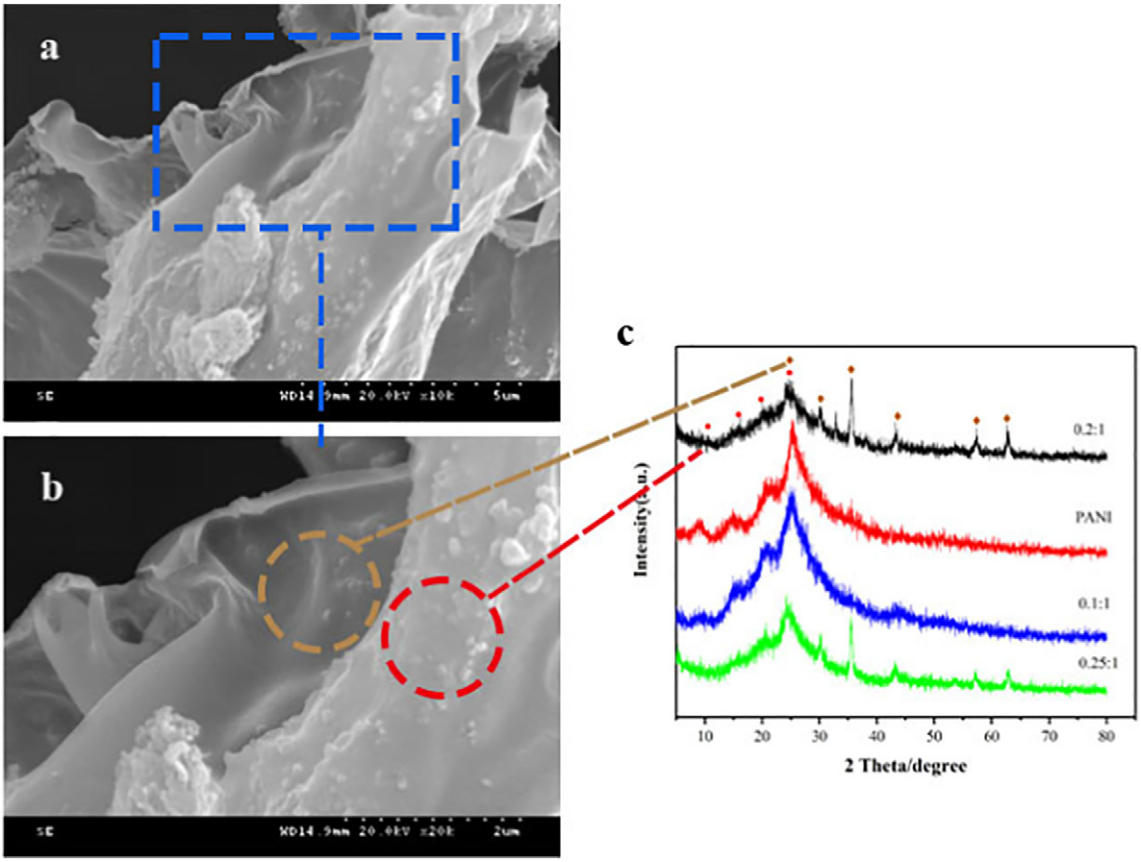

Fig. 1. SEM images of a and b: PANI/MG; XRD images of c: PANI and PANI/MG (MG:PANI = 0.1:1, 0.2:1 and 0.25:1).

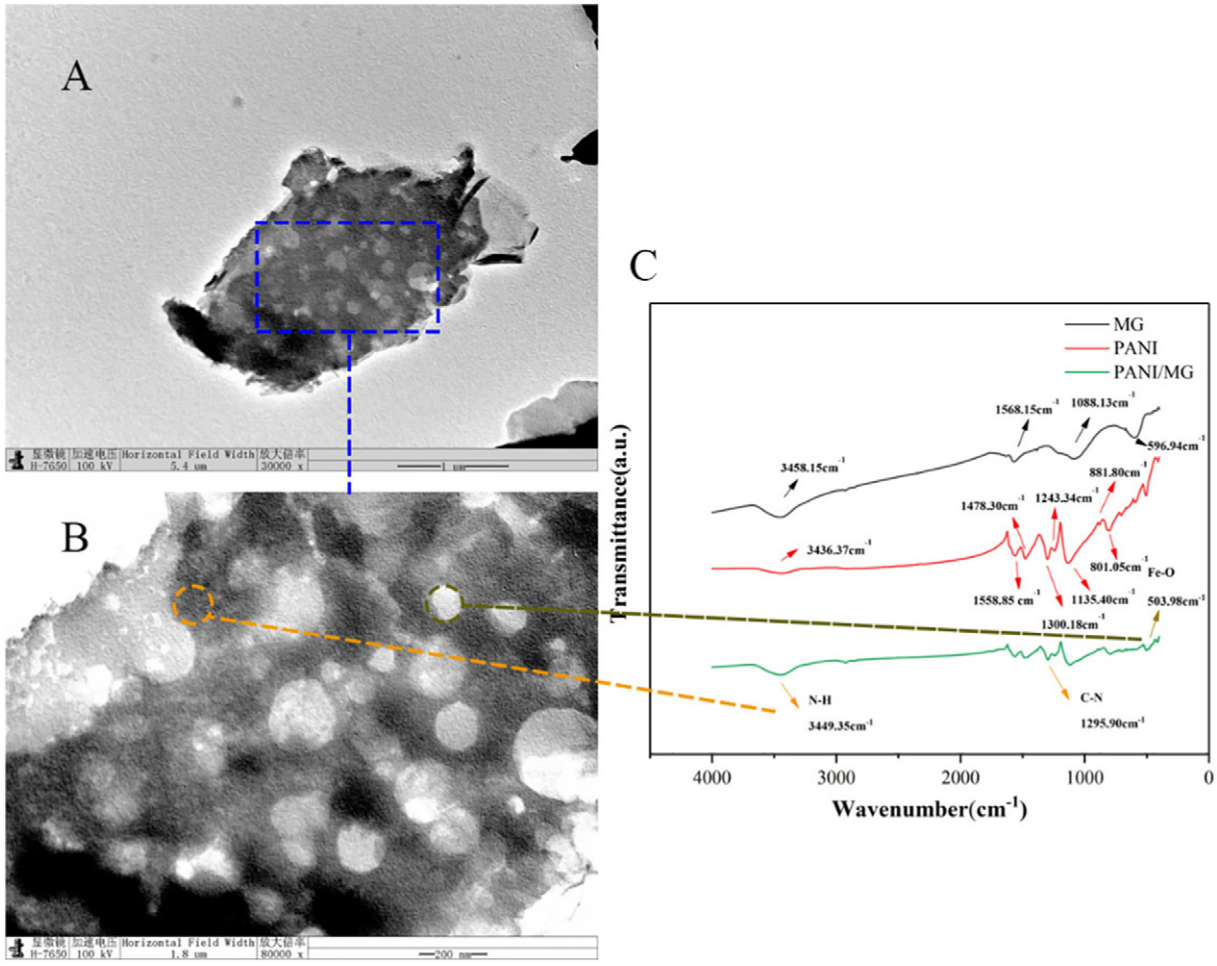

Fig. 2. TEM images of a and b: PANI/MG; FI-IR images of c:MG, PANI and PANI/MG.

changes in current value with substrate concentration. These two methods were applied for evaluating the electrochemical performance of the biosensors. The experimental voltage of chronoamperometry technology was at 0.6 V.

3. Results and discussion

3.1. Characterizations

The morphologies of PANI/MG were observed by SEM and TEM, Fig. 1a&b and Fig. 2a&b. For the three-dimension graphene-Fe_3O_4-

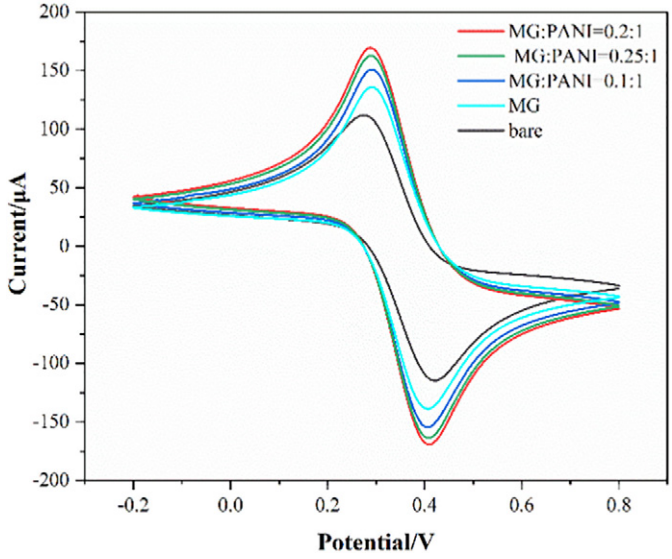

Fig. 3. Cyclic voltammetry curve (CV) of GCE, MG and PANI/MG(MG:PANI = 0.1:1, 0.2:1 and 0.25:1).

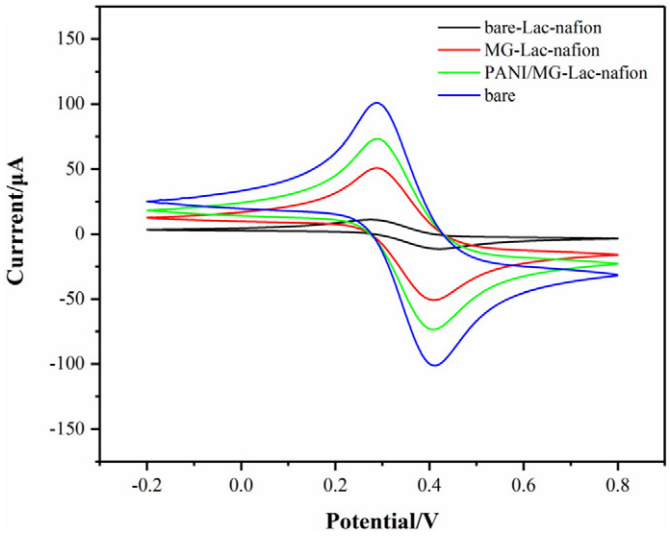

Fig. 4. Cyclic voltammetry curves (CV) of GCE, Lac-GCE, MG-Lac-GCE and PANI/MG-Lac-GCE.

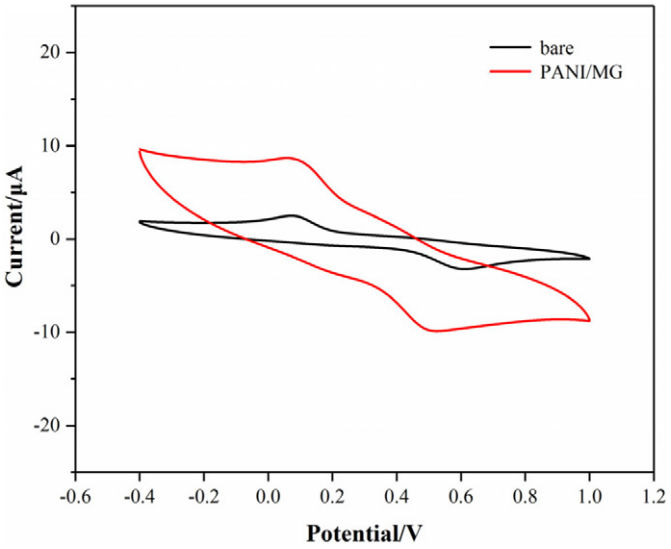

Fig. 5. Cyclic voltammetry (CV) curves of GCE and PANI/MG-Lac-GCE containing 50 μM hydroquinone (HQ) at pH 5.0.

PANI, it can be clearly seen from the SEM image (Fig. 1a&b) that polyaniline is supported on the surface of magnetic graphene, and Fe_3O_4 NPs are supported on the surface of graphene. The three-dimensional structure of the material was thus obtained. A number of nano-cavities displayed in the TEM image (Fig. 2a&b) are due to the even distribution of Fe_3O_4 where are covered with polyaniline and supported on the graphene sheets, which further explains the spatial structure of formed composites.

The component of PANI/MG was characterized by XRD, Fig. 1c. The peaks at 2θ = 15.86°, 22.31°, 25.64° correspond to the (011), (020), and (200) crystal plane characteristic diffraction peaks of PANI [68]. It can be seen that PANI and the composites of 0.1:1 displayed the above diffraction peaks, but in the case of 0.1:2, the intensity of the diffraction peak was lowered, possibly due to a decrease in the mass ratio. In the composites of 0.1:2, the peaks at 2θ = 18.9°, 30.2°, 35.5°, 57.2° and 62.9° correspond to (111), (200), (311), (400), (511) and (400) diffraction peaks of Fe_3O_4 [69,70], respectively. It indicates the presence of Fe_3O_4. In the composites of 0.1:1, the diffraction peak of Fe_3O_4 nanoparticles did not appear. The reason may be that under the condition of 0.1:1, the amount of polyaniline is relatively large, and Fe_3O_4 NPs are completely covered.

The chemical structure of PANI/MG (MG:PANI = 0.1:2) was further characterized by FTIR, Fig. 2c. The absorption peak of MG at 3458.15 cm^{-1} is caused by the hydroxyl groups [71], but its peak intensity is weak, indicating that the surface hydroxyl group of graphene oxide is reduced. The absorption peaks at 1088.13 cm^{-1} and 1568.15 cm^{-1} are the stretching vibrations of the C—O and C═C bonds of the epoxy group [72]. The absorption peak at 596.64 cm^{-1} due to the Fe—O bond [71] further confirms the existence of Fe_3O_4.

The —NH and C═C stretching vibration absorption peaks in the polyaniline appear at 3436.37 cm^{-1}, 1558.85 $cm^{-1}$and 1478.30 cm^{-1} respectively [73]. The peaks at 1300.18 cm^{-1} and 1243.34 cm^{-1} correspond to the C—N stretching vibration in the benzene ring [74]. The one at 1135.40 cm^{-1} is due to the C—H bending vibration [73]. The C—H out-of-plane bending vibration absorption peak is displayed at 881.8 cm^{-1} [75]. The absorption peak at 801.05 cm^{-1} is the C—H in-plane deformation vibration in the tetra-substituted benzene ring [76], which proves the synthesis of polyaniline. The corresponding characteristic peaks appear on the PANI/MG samples, but the intensity and position have slight changes. These indicate the interaction between PANI and MG. PANI/MG has an N—H stretching vibration peak at 3449.35 cm^{-1} [75], a C—N stretching vibration peak at 1295.90 cm^{-1} [77], and an absorption peak of Fe—O bond in MG at 503.98 cm^{-1} [78]. The results further demonstrate the synthesis of PANI/MG.

3.2. Electrocatalysis of the PANI/MG/GCE

Fig.3 shows that the cyclic voltammetry curve (CV) of a glassy carbon electrode (GCE), and the PANI/MG modified electrode with different mass ratios. It can be seen that the PANI/MG composites have a good electrical conductivity and has a higher electrical performance than the glassy carbon electrode. In the optimization of the carrier, it can be seen that when the mass ratio of MG: PANI is 0.1:2, the conductivity is optimal. When the mass ratio of MG: PANI is 0.1:2.5, the conductivity is decreased. The reason may be that the less proportion of polyaniline affects its conductivity.

Fig. 4 shows the cyclic voltammetry curve for the GCE, Lac-GCE, MG-Lac-GCE and PANI/MG-Lac-GCE. It can be seen that each electrode has an excellent redox reversibility, and the Lac-GCE peak current is significantly lower than the GCE current, which is due to the fact that Lac acts as a non-conducting protein, affecting the electron transfer. The peak current of PANI/MG-Lac-GCE is improved relative to the MG-Lac-GC and it is much higher than Lac-GCE, indicating that PANI/MG accelerates electron transfer and improves the electrocatalytic performance of the biosensor. Fig. 5 shows the current response of a GCE, PANI/MG-Lac-

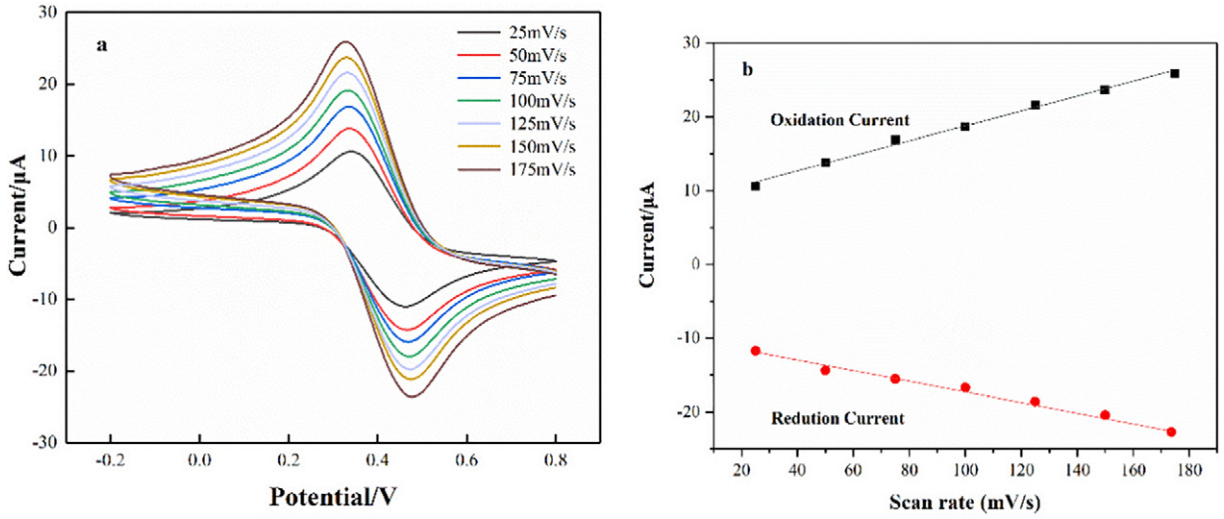

Fig. 6. Cyclic voltammetry (CV) curves of different scan rate of PANI/MG-Lac-GCE at pH 5.0 (a) and the relationship between peak current values and scan rate (b).

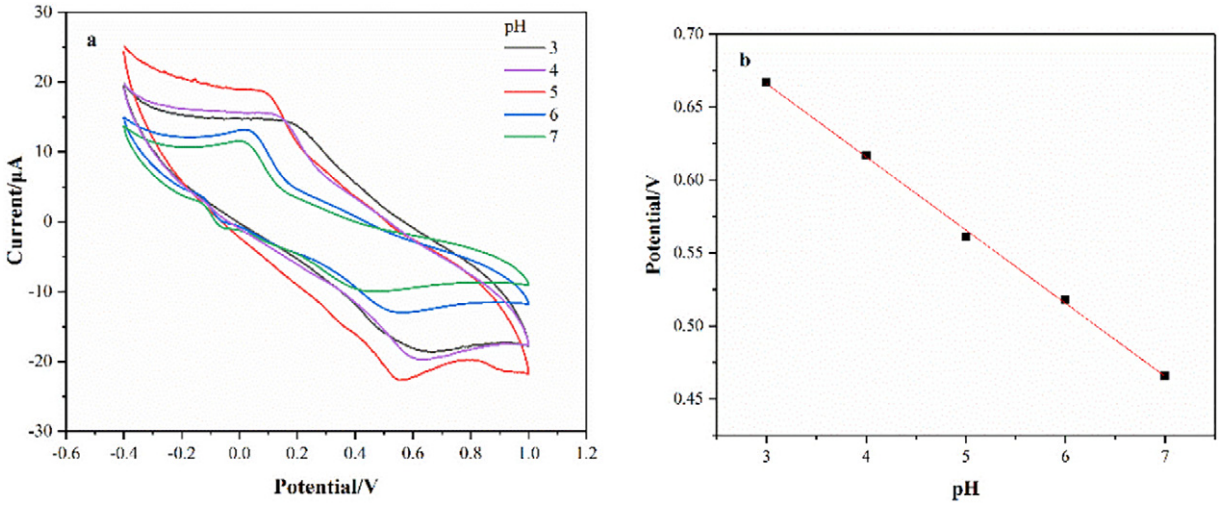

Fig. 7. Cyclic voltammetry curve (CV) of PANI/MG-Lac-GCE at a scan rate of 100 mV/s for different pH of 50 μM HQ (a) and the relationship between oxidation peak potential and pH (b).

GCE electrode in a cyclic voltammetry test of 50 μM hydroquinone (HQ) in pH 5.0 buffer. It can be seen that the peak current of Lac-PANI/MG/GCE is greatly improved, indicating that the composite material has a direct electrochemical activity and accelerates the electron transfer of the enzyme. Besides, the difference of the redox peak potential decreases (ΔE_p decreases), indicating that laccase has a good catalytic activity for HQ.

Fig. 6 shows the cyclic voltammetry and the relationship between the peak current and the scan rate of the PANI/MG-Lac-GCE in a buffer solution of pH 5.0. As shown in Fig. 6, with increasing the scan rate, the oxidation and peak and reduction peak currents also have a favorable linear relationship by the linear fitting of peak current values. It can be reasonably assumed that the electrode reaction is a surface-controlled quasi-reversible process [68].

Fig. 7 shows the cyclic voltammetry and the relationship between the peak current and the pH of PANI/MG-Lac-GCE containing 50 μM hydroquinone (HQ) phenol in buffer solution with different pH values. It can be seen that in the range of pH 3.0–7.0, the peak current increases first and then decreases with the change of pH, and the peak current reaches the maximum at pH 5.0. Besides, it can be seen that the potential of the oxidation peak has a favorable linear relationship with changing the pH. It is indicated that the protons in the reaction process of PANI/MG-Lac-GCE participate in the main process. Protons participate in the reduction process of laccase and combine with O_2 to form water as shown in Eqs. (1) and (2) [74,76]:

$$HQ + O_2 \xrightarrow{\text{laccase}} 1,4-\text{benzoquinone} + 2H_2O \quad (1)$$

$$1,4-\text{benzoquinone} + 2e^- + 2H^+ \rightarrow HQ \quad (2)$$

Fig. 8a shows the chronoamperometry of PANI/MG-Lac-GCE in the addition of HQ under stirring. It can be seen that as the concentration of HQ increases, the response current of the PANI/MG-Lac-GCE electrode increases. It can be seen that when HQ is added to the system, the current responds quickly and is stabilized rapidly within 5 s, indicating that the biosensor has an excellent current response to HQ. By calculating the average value of the steady current after each addition of HQ, it can be seen that the response current value of the electrode varies with HQ concentration in Fig. 8b. The increase is in a favorable linear relationship. The linear range of the biosensor is 0.4–337 μM, the linear equation is: $I = 0.03647c + 0.09816$, the R^2 is 0.998, the sensitivity is 36.47 μA/mM, and the detection limit is 2.94 μM. A comparison of the biosensor with the hydroquinone biosensor reported in recent years is shown in Table 1 [79–83]. It can be seen from the Table that the

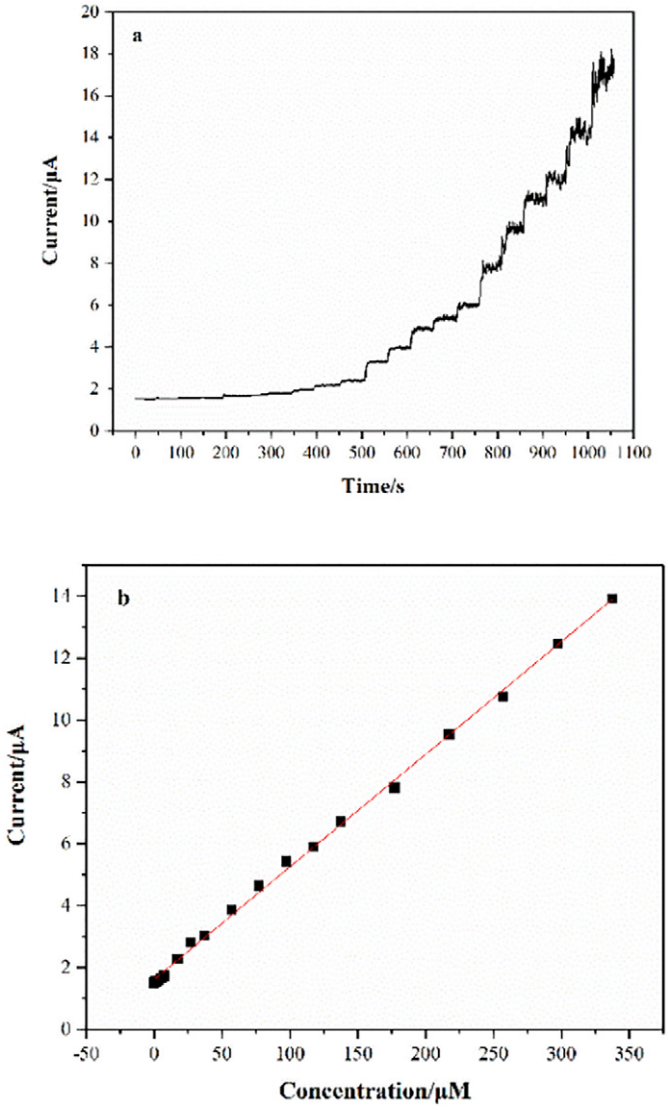

Fig. 8. Chronoamperometry of PANI/MG-Lac-GCE continuously added to HQ: Amperometric response of PANI/MG-Lac- GCE with different concentrations of HQ (a), calibration curve of the current values vs concentration of HQ (b).

Table 1
Comparison of hydroquinone biosensors.

Electrode description	Detection limit (μM)	Linear range (μM)	Sensitivity (μA/mM)	Reference
AP-rGOs/Chit/GCE	2	3–2000	14.16	67
Fe_3O_4-SiO_2/CPE	0.015	0.1–137.5	–	68
OMC–Au/L-lysine/Au/GCE	0.05	0.4–80	–	69
TiO2-CuCNFs/GCE	3.65	1–89.8	24.6	70
Si4Pic + Cl-/CPE	10	10–450	66	71
PANI/MG/GCE	2.94	0.4–337.2	36.47	This work

prepared biosensor has a satisfactory linear range and sensitivity, which proves the excellent biocompatibility and conductivity of the PANI/MG composites.

The phenols were tested 5 times with the same modified electrode in a buffer solution containing 5 μM hydroquinone, and the relative standard deviation (RSD) of the test results was 3.7%. Three modified electrodes were prepared in the same methods and measured for a buffer solution of 5 μM hydroquinone. The response current shows a relative standard deviation of 4.3%. In the 5 μM hydroquinone solution, after 20 cycles of the modified electrode, the current only changed 1.9%. After the biosensor was stored at 4 °C for 2 weeks, the same concentration of phenol was detected, and the response current was observed, and the current was reduced by 3.3%. The above results indicate that the modified electrode has the merits of excellent repeatability, reproducibility and stability.

The biosensor detected the water sample of adjusting laboratory tap water to pH 5.0. The same batch of water sample was continuously measured five times, and the RSD was calculated to be 2.57%. The measured value and the true value were calculated from the linear relationship between the current and the concentration shown in Fig.8, and the recoveries (the percentage of the detection value to the real value) (Table 2) are calculated to be between 97.125% and 103.10%, indicating that the biosensor has a good recovery rate and can be applied to detect HQ in real sample.

Fig. 9 shows the anti-interference repeatability and stability test of PANI/MG-Lac-GCE. An interference substance equivalent to HQ was added to a pH 5.0 buffer of 5 μM HQ and compared with the initial current. The response current did not change too much. It shows that the PANI/MG-Lac-GCE has excellent catalytic performance and selectivity for HQ.

4. Conclusion

The biosensor of PANI/MG-Lac-GCE was prepared via synthesizing polyaniline/magnetic graphene nanocomposites and immobilizing the biomolecule laccase. The results show that PANI/MG-Lac-GCE biosensor has a low detection limit, excellent selectivity, repeatability, reproducibility and stability. Its electrocatalytic effect on hydroquinone (HQ) proves that the prepared biosensor is a prospective phenolic biosensor for real water applications.

Declaration of competing interest

There is no conflict of interests for this submission.

Table 2
Determination of HQ content in tap water samples.

Sample	Real value μmol/L	Detection value μmol/L	Recovery %	Relative standard deviation %
1	7.20	7.341	101.94	2.57
		7.219	100.26	
		7.423	103.10	
		7.043	97.82	
		6.993	97.125	

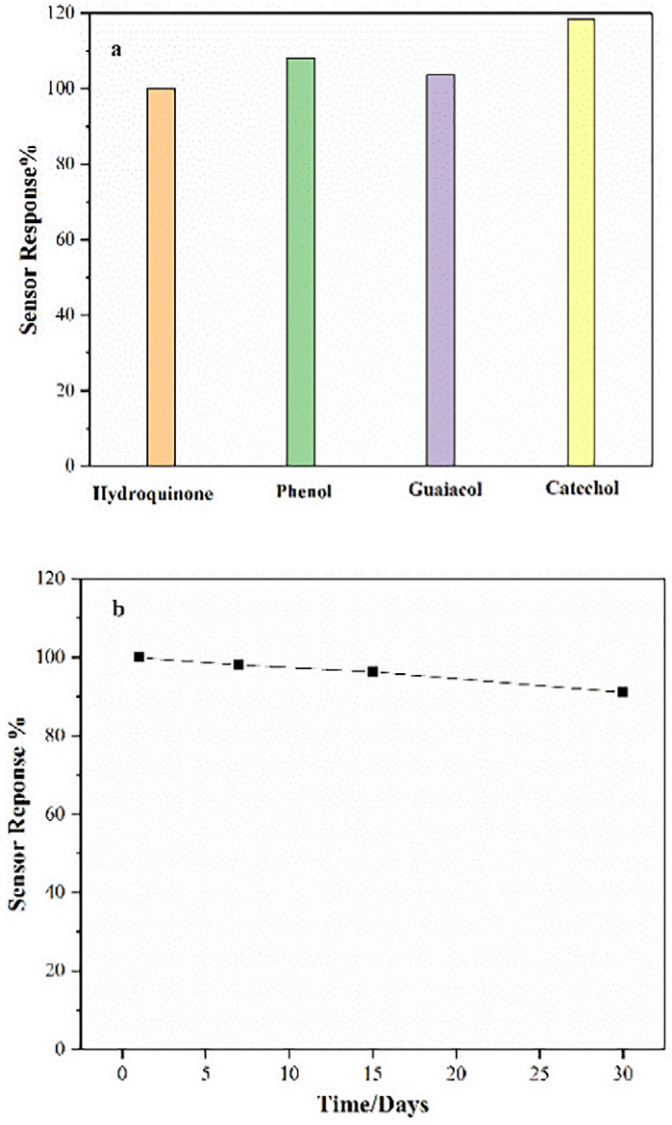

Fig. 9. The anti-interference of PANI/MG-Lac-GCE.in a pH 5.0 buffer of 5 μM HQ containing different phenolic compounds (a); the stability of PANI/MG-Lac-GCE saved for one month at 4 °C.

All authors agreed on this submission.
The paper is not considered by any other journal at this moment.

Acknowledgement

The authors are grateful for the Project supported by the Graduate innovation research projects for Qiqihar University (Item No.: YJSCX2018-030X) and Project supported by reserve leaders of Heilongjiang provincial leading talent echelon.

References

[1] Y. Wee, S. Park, Y.H. Kwon, Y. Ju, K.-M. Yeon, J. Kim, Tyrosinase-immobilized CNT based biosensor for highly-sensitive detection of phenolic compounds, Biosens. Bioelectron. 132 (2019) 279–285.
[2] M.M. Rodríguez-Delgado, G.S. Alemán-Nava, J.M. Rodríguez-Delgado, G. Dieck-Assad, S.O. Martínez-Chapa, D. Barceló, R. Parra, Laccase-based biosensors for detection of phenolic compounds, Trac Trends in Analytical Chem 74 (2015) 21–45.
[3] F.M. Fartas, J. Abdullah, N.A. Yusof, Y. Sulaiman, M.I. Saiman, Biosensor based on tyrosinase immobilized on graphene-decorated gold nanoparticle/chitosan for phenolic detection in aqueous, Sensors 17 (5) (2017) 1132.
[4] A. Boujakhrout, S. Jimenez-Falcao, P. Martínez-Ruiz, A. Sánchez, P. Díez, J.M. Pingarrón, R. Villalonga, Novel reduced graphene oxide-glycol chitosan nanohybrid

for the assembly of an amperometric enzyme biosensor for phenols, Analyst 141 (13) (2016) 4162.
[5] E. Han, Y. Yang, Z. He, J. Cai, X. Zhang, X. Dong, Development of tyrosinase biosensor based on quantum dots/chitosan nanocomposite for detection of phenolic compounds, Anal. Biochem. 486 (2015) 102–106.
[6] Y. Zou, L. Dong, D. Kang, L. He, Y. Dong, S. Wang, Amperometric tyrosinase biosensor based on boron-doped nanocrystalline diamond film electrode for the detection of phenolic compounds, J. Solid State Electrochem. 20 (1) (2016) 47–54.
[7] M.A. Rodríguez-Delgado, S. Malovaná, J.P. Pérez, T. Borges, F.J. Montelongo, García, separation of phenolic compounds by high-performance liquid chromatography with absorbance and fluorimetric detection, J. Chromatography A 912 (2) (2001) 249–257.
[8] I.K. Bae, H.M. Ham, H.J. Min, H.K. Dong, H.J. Kim, Simultaneous determination of 15 phenolic compounds and caffeine in teas and mate using RP-HPLC/UV detection: method development and optimization of extraction process, Food Chem. 172 (2015) 469–475.
[9] C. Proestos, D. Sereli, M. Komaitis, Determination of phenolic compounds in aromatic plants by RP-HPLC and GC-MS, Food Chemm 95 (1) (2006) 44–52.
[10] M. Govindhan, T. Lafleur, B.a. Adhikari, A. Chen, Electrochemical sensor based on carbon nanotubes for the simultaneous detection of phenolic pollutants, Electroanalysis 27 (4) (2015) 902–909.
[11] Q. Yang, X. Wu, H. Peng, L. Fu, X. Song, J. Li, H. Xiong, L. Chen, Q. Yang, X. Wu, Simultaneous phase-inversion and imprinting based sensor for highly sensitive and selective detection of bisphenol a, Talanta 176 (2017) 595–603.
[12] G. Zhang, L. Fang, F. Li, B. Gao, Surface molecularly imprinted electrochemical sensor for phenol based on SiO_2 nanoparticles, RSC Adv. 6 (2016) 56936–56943.
[13] C.C. Mayorga-Martinez, R. Gusmão, Z. Sofer, M. Pumera, Pnictogen-based enzymatic phenol biosensors: phosphorene, arsenene, antimonene, and bismuthene, Ang. Chem. Inter. Ed. 58 (1) (2019) 134–138.
[14] L.P. Mei, J.J. Feng, L. Wu, J.Y. Zhou, J.R. Chen, A.J. Wang, Novel phenol biosensor based on laccase immobilized on reduced graphene oxide supported palladium–copper alloyed nanocages, Biosens. Bioelectron. 74 (2015) 347–352.
[15] M. Nazari, S. Kashanian, R. Rafipour, Laccase immobilization on the electrode surface to design a biosensor for the detection of phenolic compound such as catechol, Spectrochim. Acta A 145 (2015) 130–138.
[16] Y. Wang, F. Zhai, Y. Hasebe, H. Jia, Z. Zhang, A highly sensitive electrochemical biosensor for phenol derivatives using a graphene oxide-modified tyrosinase electrode, Bioelectrochem 122 (2018) 174–182.
[17] M. Liu, Q. Meng, Z. Yang, X. Zhao, T. Liu, Ultra-long-term cycling stability of an integrated carbon–sulfur membrane with dual shuttle-inhibiting layers of graphene "nets" and a porous carbon skin, Chem. Commun. 54 (40) (2018) 5090–5093.
[18] L. Ma, Y. Zhu, P. Feng, G. Song, Y. Huang, H. Liu, J. Zhang, J. Fan, H. Hou, Z. Guo, Reinforcing carbon fiber epoxy composites with triazine derivatives functionalized graphene oxide modified sizing agent, Compo. Part B. 176 (2019) 107078.
[19] Y.X. Qian, Y.H. Yuan, H.L. Wang, H. Liu, J.X. Zhang, S. Shi, Z.H. Guo, N. Wang, Highly efficient uranium adsorption by salicylaldoxime/polydopamine graphene oxide nanocomposites, J. Mater. Chem. A 6 (48) (2018) 24676–24685.
[20] G. Zhu, X. Cui, Y. Zhang, S. Chen, M. Dong, H. Liu, Q. Shao, T. Ding, S. Wu, Z. Guo, Poly (vinyl butyral)/Graphene oxide/poly (methylhydrosiloxane) nanocomposite coating for improved aluminum alloy anticorrosion, Polymer 172 (2019) 415–422.
[21] V. Murugadoss, J. Lin, H. Liu, X.M. Mai, T. Ding, Z.H. Guo, S. Angaiah, Optimizing graphene content in a NiSe/graphene nanohybrid counter electrode to enhance the photovoltaic performance of dye-sensitized solar cells, Nanoscale 11 (38) (2019) 17579–17589.
[22] J. Zhang, W. Zhang, L. Wei, L. Pu, J. Liu, H. Liu, Y. Li, J. Fan, T. Ding, Z. Guo, Alternating multilayer structural epoxy composite coating for corrosion protection of steel, Macromol. Mater. Eng. 304 (12) (2019), 1900374.
[23] J.X. Zhang, P.P. Li, Z.Z. Zhang, X.J. Wang, J.J. Tang, H. Liu, Q. Shao, T. Ding, A. Umar, Z.H. Guo, Solvent-free graphene liquids: promising candidates for lubricants without the base oil, J. Colloid Interface Sci. 542 (2019) 159–167.
[24] K. Sun, J.N. Dong, Z.X. Wang, Z.Y. Wang, G.H. Fan, Q. Hou, L.Q. An, M.Y. Dong, R.H. Fan, Z.H. Guo, Tunable negative permittivity in flexible graphene/PDMS metacomposites, J. Phys. Chem. C 123 (38) (2019) 23635–23642.
[25] K. Le, Z. Wang, F. Wang, Q. Wang, Q. Shao, V. Murugadoss, S. Wu, W. Liu, J. Liu, Q. Gao, Z. Guo, Sandwich-like NiCo layered double hydroxide/reduced graphene oxide nanocomposite cathodes for high energy density asymmetric supercapacitors, Dalton Trans. 48 (16) (2019) 5193–5202.
[26] M. Idrees, S. Batool, J. Kong, Q. Zhuang, H. Liu, Q. Shao, N. Lu, Y. Feng, E.K. Wujcik, Q. Gao, T. Ding, R. Wei, Z. Guo, Polyborosilazane derived ceramics - nitrogen sulfur dual doped graphene nanocomposite anode for enhanced lithium ion batteries, Electrochim. Acta 296 (2019) 925–937.
[27] Y. Guo, X. Yang, K. Ruan, J. Kong, M. Dong, J. Zhang, J. Gu, Z. Guo, Reduced graphene oxide heterostructured silver nanoparticles significantly enhanced thermal conductivities in hot-pressed electrospun polyimide nanocomposites, ACS Appl. Mater. Interfaces 11 (28) (2019) 25465–25473.
[28] B. Kirubasankar, V. Murugadoss, J. Lin, T. Ding, M. Dong, H. Liu, J. Zhang, T. Li, N. Wang, Z. Guo, S. Angaiah, In situ grown nickel selenide on graphene nanohybrid electrodes for high energy density asymmetric supercapacitors, Nanoscale 10 (43) (2018) 20414–20425.
[29] X. Huang, R. Yin, L. Qian, W. Zhao, H. Liu, C. Liu, J. Fan, H. Hou, J. Zhang, Z. Guo, Processing conditions dependent tunable negative permittivity in reduced graphene oxide-alumina nanocomposites, Ceram. Int. 45 (14) (2019) 17784–17792.
[30] K. Sun, J.H. Xin, Z.X. Wang, S. Feng, Z.Y. Wang, R.H. Fan, H. Liu, Z.H. Guo, Weakly negative permittivity and low frequency dispersive behavior in graphene/epoxy metacomposites, J. Mater. Sci. 30 (15) (2019) 14745–14754.
[31] Y. Zhang, Y. An, L. Wu, H. Chen, Z. Li, H. Dou, V. Murugadoss, J. Fan, X. Zhang, X. Mai, Z. Guo, Metal-free energy storage systems: combining batteries with capacitors based on a methylene blue functionalized graphene cathode, J. Mater. Chem. A 7 (34) (2019) 19668–19675.
[32] S.W. Li, P.P. Yang, X.H. Liu, J.X. Zhang, W. Xie, C. Wang, C.T. Liu, Z.H. Guo, Graphene oxide based dopamine mussel-like cross-linked polyethylene imine nanocomposite coating with enhanced hexavalent uranium adsorption, J. Mater. Chem. A 7 (28) (2019) 16902–16911.
[33] X. Gong, Y. Liu, Y. Wang, Z. Xie, Q. Dong, M. Dong, H. Liu, Q. Shao, N. Lu, V. Murugadoss, T. Ding, Z. Guo, Amino graphene oxide/dopamine modified aramid fibers: preparation, epoxy nanocomposites and property analysis, Polymer 168 (2019) 131–137.
[34] Y.X. He, Q.Y. Chen, H. Liu, L. Zhang, D.Y. Wu, C. Lu, W. OuYang, D.F. Jiang, M.F. Wu, J.X. Zhang, Y.C. Li, J.C. Fan, C.T. Liu, Z.H. Guo, Friction and wear of MoO_3/graphene oxide modified glass fiber reinforced epoxy nanocomposites, Macromol. Mater. Eng. 304 (8) (2019) 1900166.
[35] S. Palanisamy, S.K. Ramaraj, S.M. Chen, T.C.K. Yang, Y.F. Pan, T.W. Chen, V. Velusamy, S. Selvam, A novel Laccase biosensor based on Laccase immobilized graphene-cellulose microfiber composite modified screen-printed carbon electrode for sensitive determination of catechol, Sci. Rep. 7 (2017) 41214.
[36] X. Liu, R. Yan, J. Zhu, J. Zhang, X. Liu, Growing TiO2 nanotubes on graphene nanoplatelets and applying the nanonanocomposite as scaffold of electrochemical tyrosinase biosensor, Sensors Actuators B Chem. 209 (2015) 328–335.
[37] M. Nazari, S. Kashanian, N. Maleki, N. Shahabadi, Laccase Immobilized onto Graphene Oxide Nanosheets and Electrodeposited Gold–Cetyltrimethylammonium Bromide Complex to Fabricate a Novel Catechol Biosensor, 42, Bulletin Mater. Sci., 2019 51.
[38] C. Lou, T. Jing, J. Tian, Y. Zheng, J. Zhang, M. Dong, C. Wang, C. Hou, J. Fan, Z. Guo, 3-dimensional graphene/Cu/Fe_3O_4 composites: immobilized laccase electrodes for detecting bisphenol A, J. Mater. Res. 34 (17) (2019) 2964–2975.
[39] R. Ma, Y. Wang, H. Qi, C. Shi, G. Wei, L. Xiao, Z. Huang, S. Liu, H. Yu, C. Teng, H. Liu, V. Murugadoss, J. Zhang, Y. Wang, Z. Guo, Nanocomposite sponges of sodium alginate/graphene oxide/polyvinyl alcohol as potential wound dressing: in vitro and in vivo evaluation, Compos. Part B 167 (2019) 396–405.
[40] Z. Zhao, P. Bai, R.D.K. Misra, M. Dong, R. Guan, Y. Li, J. Zhang, L. Tan, J. Gao, T. Ding, W. Du, Z. Guo, AlSi10Mg alloy nanocomposites reinforced with aluminum-coated graphene: selective laser melting, interfacial microstructure and property analysis, J. Alloys Compounds 792 (2019) 203–214.
[41] W. Deng, T. Kang, H. Liu, J. Zhang, N. Wang, N. Lu, Y. Ma, A. Umar, Z. Guo, Potassium hydroxide activated and nitrogen doped graphene with enhanced supercapacitive behavior, Sci. Adv. Mater. 10 (7) (2018) 937–949.
[42] H. Beitollahi, S. Tajik, S. Jahani, Electrocatalytic determination of hydrazine and phenol using a carbon paste electrode modified with ionic liquids and magnetic core-shell Fe_3O_4@ SiO_2/MWCNT nanocomposite, Electroanalysis 28 (5) (2016) 1093–1099.
[43] M. Dervisevic, E. Custiuc, E. Çevik, Z. Durmus, M. Şenel, A. Durmus, Electrochemical biosensor based on REGO/Fe 3 O 4 bionanocomposite interface for xanthine detection in fish sample, Food Control 57 (2015) 402–410.
[44] N. Sanaeifar, M. Rabiee, M. Abdolrahim, M. Tahriri, D. Vashaee, L. Tayebi, A novel electrochemical biosensor based on Fe_3O_4 nanoparticles-polyvinyl alcohol composite for sensitive detection of glucose, Anal. Biochem. 519 (2016) 19.
[45] T.-T. Xia, C.-Z. Liu, J.-H. Hu, C. Guo, Improved performance of immobilized laccase on amine-functioned magnetic Fe_3O_4 nanoparticles modified with polyethylenimine, Chem. Eng. J. 295 (2016) 201–206.
[46] H. Gu, X. Zhou, S. Lyu, D. Pan, M. Dong, S. Wu, T. Ding, X. Wei, I. Seok, S. Wei, Z. Guo, Magnetic nanocellulose-magnetite aerogel for easy oil adsorption, J. Colloid Interface Sci. 560 (2020) 849–856.
[47] J. Guo, H. Song, H. Liu, C. Luo, Y. Ren, T. Ding, M.A. Khan, D.P. Young, X. Liu, X. Zhang, J. Kong, Z. Guo, Polypyrrole-interface-functionalized nano-magnetite epoxy nanocomposites as electromagnetic wave absorbers with enhanced flame retardancy, J. Mater. Chem. C 5 (22) (2017) 5334–5344.
[48] Y.Y. Li, T. Jing, G.F. Xu, J.Z. Tian, M.Y. Dong, Q. Shao, B. Wang, Z.K. Wang, Y.J. Zheng, C.L. Yang, Z.H. Guo, 3-D magnetic graphene oxide-magnetite poly(vinyl alcohol) nanocomposite substrates for immobilizing enzyme, Polymer 149 (2018) 13–22.
[49] M. Liu, B. Li, H. Zhou, C. Chen, Y. Liu, T. Liu, Extraordinary rate capability achieved by a 3D "skeleton/skin" carbon aerogel–polyaniline hybrid with vertically aligned pores, Chem. Commun. 53 (19) (2017) 2810–2813.
[50] X. Xu, Q. Fu, H. Gu, Y. Guo, H. Zhou, J. Zhang, D. Pan, S. Wu, M. Dong, Z. Guo, Polyaniline crystalline nanostructures dependent negative permittivity metamaterials, Polymer 188 (2020), 122129.
[51] H. Gu, X. Xu, J. Cai, S. Wei, H. Wei, H. Liu, D.P. Young, Q. Shao, S. Wu, T. Ding, Z. Guo, Controllable organic magnetoresistance in polyaniline coated poly(p-phenylene-2,6-benzobisoxazole) short fibers, Chem. Commun. 55 (68) (2019) 10068–10071.
[52] Y. Ma, Z. Zhuang, M. Ma, Y. Yang, W. Li, J. lin, M. Dong, S. Wu, T. Ding, Z. Guo, Solid polyaniline dendrites consisting of high aspect ratio branches self-assembled using sodium lauryl sulfonate as soft templates: synthesis and electrochemical performance, Polymer 182 (2019), 121808.
[53] Y. Ma, C. Hou, H. Zhang, Q. Zhang, H. Liu, S. Wu, Z. Guo, Three-dimensional core-shell Fe_3O_4/polyaniline coaxial heterogeneous nanonets: preparation and high performance supercapacitor electrodes, Electrochim. Acta 315 (2019) 114–123.
[54] Q. Hu, N. Zhou, K. Gong, H. Liu, Q. Liu, D. Sun, Q. Wang, Q. Shao, H. Liu, B. Qiu, Z. Guo, Intracellular polymer substances induced conductive polyaniline for improved methane production from anaerobic wastewater treatment, ACS Sustain. Chem. Eng. 7 (6) (2019) 5912–5920.
[55] Y. Ma, M.L. Ma, X.Q. Yin, Q. Shao, N. Lu, Y.N. Feng, Y. Lu, E.K. Wujcik, X.M. Mai, C. Wang, Z.H. Guo, Tuning polyaniline nanostructures via end group substitutions

and their morphology dependent electrochemical performances, Polymer 156 (2018) 128–135.
[56] H.B. Gu, H.Y. Zhang, J. Lin, Q. Shao, D.P. Young, L.Y. Sun, T.D. Shen, Z.H. Guo, Large negative giant magnetoresistance at room temperature and electrical transport in cobalt ferrite-polyaniline nanocomposites, Polymer 143 (2018) 324–330.
[57] K.D. Gong, Q. Hu, Y.Y. Xiao, X. Cheng, H. Liu, N. Wang, B. Qiu, Z.H. Guo, Triple layered core-shell ZVI@carbon@polyaniline composite enhanced electron utilization in Cr (vi) reduction, J. Mater. Chem. A 6 (24) (2018) 11119–11128.
[58] K.D. Gong, S.Y. Guo, Y. Zhao, Q. Hu, H. Liu, D.Z. Sun, M. Li, B. Qiu, Z.H. Guo, Bacteria cell templated porous polyaniline facilitated detoxification and recovery of hexavalent chromium, J. Mater. Chem. A 6 (35) (2018) 16824–16832.
[59] H. Zheng, Z. Yan, M. Wang, J. Chen, X. Zhang, Biosensor based on polyaniline-polyacrylonitrile-graphene hybrid assemblies for the determination of phenolic compounds in water samples, J. Hazar. Mater. 378 (2019), 120714.
[60] M. Oves, M. Shahadat, S. Ansari, M. Aslam, in: A. Khan, M. Jawaid, A.A.P. Khan, A.M. Asiri (Eds.), Polyaniline Nanocomposite Materials for Biosensor Designing. In Electrically Conductive Polymer and Polymer Composites: From Synthesis to Biomedical Applications, Wiley-VCH Verlag, Weinheim, Germany 2018, pp. 113–135.
[61] J.H. Kim, S.G. Hong, H.J. Sun, H. Su, J. Kim, Precipitated and chemically-crosslinked laccase over polyaniline nanofiber for high performance phenol sensing, Chemosphere 143 (2016) 142–147.
[62] Q. Dong, X. Wang, H. Liu, H. Ryu, J. Zhao, B. Li, Y. Lei, Heterogeneous iridium oxide/gold nanocluster for non-enzymatic glucose sensing and pH probing, Eng. Sci. 8 (2019) 46–53, https://doi.org/10.30919/es8d512(In this issue).
[63] S.K.S. Patel, M.Z. Anwar, A. Kumar, S.V. Otari, R.T. Pagolu, S.Y. Kim, I.W. Kim, J.K. Lee, Fe_2O_3 yolk-shell particle-based laccase biosensor for efficient detection of 2,6-dimethoxyphenol, Biochem. Eng. J. 132 (2018) 1–8.
[64] Y. Zheng, D. Wang, Z. Li, X. Sun, T. Gao, G. Zhou, Laccase biosensor fabricated on flower–shaped yolk–shell SiO_2 nanospheres for catechol detection, Colloids Surf. A: Physicochem. Eng. Aspects 538 (2018) 202–209.
[65] M. Romero-Arcos, M.G. Garnica-Romo, H.E. Martinez-Flores, G. Vázquez-Marrufo, R. Ramírez-Bon, J. González-Hernández, G.V. Barbosa-Cánovas, Enzyme immobilization by amperometric biosensors with TiO_2 nanoparticles used to detect phenol compounds, Food Eng. Rev. 8 (2) (2016) 235–250.
[66] S.A.R. Albayati, S. Kashanian, M. Nazari, S. Rezaei, Novel fabrication of a laccase biosensor to detect phenolic compounds using a carboxylated multiwalled carbon nanotube on the electropolymerized support, Bull. Mater. Sci. 42 (4) (2019) 187.
[67] N. Zaaba, K. Foo, U. Hashim, S. Tan, W.-W. Liu, C. Voon, Synthesis of graphene oxide using modified hummers method: solvent influence, Procedia Eng 184 (2017) 469–477.
[68] X.W. Zheng, H.T. Yu, R.G. Xing, X. Ge, H. Sun, R.H. Li, Q.W. Zhang, Multi-growth site graphene/polyaniline composites with highly enhanced specific capacitance and rate capability for supercapacitor application, Electrochim. Acta 260 (2018) 504–513.
[69] K.F. Zhou, Y.H. Zhu, X.L. Yang, C.Z. Li, Preparation and application of mediator-free H_2O_2 biosensors of graphene-Fe_3O_4 composites, Electroanalysis 23 (4) (2011) 862–869.
[70] Y. Yang, Y.R. Zhao, S.H. Sun, X.Y. Zhang, L.F. Duan, X. Ge, W. Lu, Self-assembled three-dimensional graphene/Fe_3O_4 hydrogel for efficient pollutant adsorption and electromagnetic wave absorption, Mater. Res. Bull. 73 (2016) 401–408.
[71] Y. Wang, X.Y. Liu, X. Xu, Y. Yang, L.H. Huang, Z.Y. He, Y.H. Xu, J.J. Chen, Z.S. Feng, Preparation and characterization of reduced graphene oxide/Fe_3O_4 nanocomposite by a facile in-situ deposition method for glucose biosensor applications, Mater. Res. Bull. 101 (2018) 340–346.
[72] A.N. Mahmoodabadi, A. Kompany, M. Mashreghi, Characterization, antibacterial and cytotoxicity studies of graphene-Fe_3O_4 nanocomposites and Fe_3O_4 nanoparticles synthesized by a facile solvothermal method, Mater. Chem. Phys. 213 (2018) 285–294.
[73] H.L. Wang, Q.L. Hao, X.J. Yang, L.D. Lu, X. Wang, Graphene oxide doped polyaniline for supercapacitors, Electrochem. Commun. 11 (6) (2009) 1158–1161.
[74] Y.J. Fu, Q. An, R.Y. Ni, Y. Zhang, Y.G. Li, H.Z. Ke, Preparation of polyaniline-encapsulated carbon/copper composite nanofibers for detection of polyphenol pollutant, Colloids Surf. A: Physicochem. Eng. Aspects 559 (2018) 289–296.
[75] G.H. Xu, D.D. Xu, J.N. Zhang, K.X. Wang, Z.M. Chen, J.F. Chen, Q. Xu, Controlled fabrication of PANI/CNF hybrid films: molecular interaction induced various micromorphologies and electrochemical properties, J. Colloid Interface Sci. 411 (2013) 204–212.
[76] Z.Y. Pang, J.P. Fu, L. Luo, F.L. Huang, Q.F. Wei, Fabrication of PA6/TiO_2/PANI composite nanofibers by electrospinning-electrospraying for ammonia sensor, Colloids Surf. A: Physicochem. Eng. Aspects 461 (2014) 113–118.
[77] Q. Xu, S.X. Gu, L.Y. Jin, Y.E. Zhou, Z.J. Yang, W. Wang, X.Y. Hu, Graphene/polyaniline/gold nanoparticles nanocomposite for the direct electron transfer of glucose oxidase and glucose biosensing, Sensors Actuators B-Chem 190 (2014) 562–569.
[78] K. Radhapyari, P. Kotoky, M.R. Das, R. Khan, Graphene-polyaniline nanocomposite based biosensor for detection of antimalarial drug artesunate in pharmaceutical formulation and biological fluids, Talanta 111 (2013) 47–53.
[79] X.H. Zhou, L.H. Liu, X. Bai, H.C. Shi, A reduced graphene oxide based biosensor for high-sensitive detection of phenols in water samples, Sensors Actuators B Chem. 181 (5) (2013) 661–667.
[80] Y. Zhang, G.M. Zeng, L. Tang, D.L. Huang, X.Y. Jiang, Y.N. Chen, A hydroquinone biosensor using modified core-shell magnetic nanoparticles supported on carbon paste electrode, Biosens. Bioelectron. 22 (9–10) (2007) 2121–2126.
[81] T. Lin, Z. Yaoyu, Z. Guangming, L. Zhen, L. Yuanyuan, Z. Yi, C. Guiqiu, Y. Guide, L. Xiaoxia, W. Mengshi, A tyrosinase biosensor based on ordered mesoporous carbon-Au/L-lysine/Au nanoparticles for simultaneous determination of hydroquinone and catechol, Analyst 138 (12) (2013) 3552.
[82] Y. Jie, D. Li, J. Fu, F. Huang, Q. Wei, TiO_2-CuCNFs based laccase biosensor for enhanced electrocatalysis in hydroquinone detection, J. Electroanalytical Chem. 766 (2016) 16–23.
[83] P.S.d. Silva, B.C. Gasparini, H.A. Magosso, A. Spinelli, Electrochemical behavior of hydroquinone and catechol at a silsesquioxane-modified carbon paste electrode, J. Brazilian Chem. Soc. 24 (4) (2013) 695–699.